SLAB AVALANCHE FORMATION, NEW MEASUREMENTS AND RESULTS

H.Gubler[1]

ABSTRACT

Three types of experiments have been started or continued during the last two years to improve our knowledge on the formation of slab avalanches: (a) Interception of snow by spruce and conditions for triggering snow fall from tree branches. (b) Modelling of energy and mass flux in a seasonal snow cover including a detailed investigation on short wave absorption in snow. (c) Field measurements of the strainrate dependent stress-strain relationship for potentially weak layers under shear stress. Experiment (a) helps to reveal the timing of snow dumping by spruce branches during periods of strong precipitation in subalpine forests. Avalanching of snow from trees may distort existing continuous weak layers, adding support to the new-snow slab by local compaction but may also trigger loose snow avalanches in steep terrain. Experiment (b) enables us to refine modelling and understanding recrystallisation processes taking place within short periods of time close to the snow surface. These fast recrystallisation processes may eventually produce weak layers whose existence is a necessary condition for slab avalanche formation. Experiment (c) for the first time allows direct measurements of the constitutive relationships for thin weak layers under shear stress. The computer controlled shear apparatus has a contact area of .25m^2 and allows measurements at constant strain rate (10^{-7} to $10^{-1}s^{-1}$) or constant stress (0 to 5000Pa). The stresses may be applied in situ on weak layers.

INTRODUCTION

Bader and Salm (1990) determined the conditions to start and propagate shear fractures in a thin weak layer within a snow-pack. They found that superweak inclusions have to form by some natural process within the continuous weak layer that interfaces the base layers of the snow pack with the slab on top. Superweak inclusions fail to transfer shear stresses from the top slab to the bottom layer. Calculations based on measurements of constitutive parameters of snow show that critical stress, strainrate and strain necessary to start propagation of a shear fracture can only be attained along the border line of superweak inclusions of some minimal size. Gubler and Bader (1989) proposed a model and interpreted field measurements that may explain natural local

[1]Swiss Federal Institute for Snow an Avalanche Research
CH-7260 Weissfluhjoch/Davos
Phone ..(0)81 46 32 64, Fax ..(0)81 46 18 97

collapses of the stress conducting structures within a weak layer. These local structural collapses or initial fractures are a necessary condition for the formation of superweak inclusions. Gubler and Rychetnik (1991) used these models to explain the conditions for the formation of slab avalanches in subalpine forests near timberline. The existence of a thin weak layer or layer interface between base layer and top slab is a necessary condition for the formation of slab avalanches. Weak layers often form close or at the surface of the snow pack by recrystallisation processes. Thin layers of facetted or featherlike crystals may form within short periods of time if high temperature gradients respective gradients of vapour density exist close to the snow surface. Structures of fast growing crystals often have very low cohesion. High local gradients result from large negative balance of infrared radiation at the snow surface and may be enhanced by absorption of solar radiation within the snow pack close to the surface. Extensive local heating of the snow structure may increase local settling and sintering or even cause subsurface melting. These are major processes for crust formation. Combinations of crusts and kinetic growth crystals including cold new snow crystals often form weak layers or layer interfaces.

Absorption of solar (short wave) radiation depends on grain size, snow density and content of impurities (mainly soot or minerals). To model and forecast these processes of weak layer formation based on measurements of short wave albedo, surface temperature, air temperature, air humidity etc., we propose a method to estimate short wave absorption close to the surface from short wave albedo measurements.

To start ductile and eventually brittle shear-fracture propagation within the weak layer strain rate and strain have to attain critical values at least locally. Under natural conditions these minimal values can only be surpassed along the border line of superweak inclusions. The dependences of strain-rate and fracture strain on stress for weak layers, base layers and slabs determine critical conditions. Therefore the minimal size of the stress concentrating superweak inclusion depends critically on these constitutive relationships. We built and tested an apparatus to measure these parameters in situ.

Bader et.al.(1988) and Gubler and Rychetnik (1991) showed that the distribution of stresses in the slab around a forest tree depends strongly on the size of the supporting area. A rim of compacted snow around the border line of the vertical projection of the crown area increases the back pressure zone significantly compared to the backpressure zone caused by the trunk only. These rims are built by precipitation particles deflected by the branches at decreasing snow-intercept efficiency of the canopy during a storm and even more efficiently by snow falling from the tree. Therefore we investigate the development of intercept efficiency and the causes for snow dumping during important precipitation events that may significantly increase slab stability and therefore decrease avalanche danger.

FUNDAMENTALS OF SLAB AVALANCHE FORMATION

The following sequence of events proved to be a plausible scenario for releases of direct-action avalanches. A necessary condition for slab fracture is the existence of a thin weak layer or a highly deformable layer interface of low cohesion between old and new snow. Shear strength and viscosity of this weak layer depend on the local structure of the snow. Weak layers normally form at or close to the surface of the snow pack. After formation, weak layers may be buried by a new slab on top during important precipitation events and/or periods of intense snow transport by wind. For the formation of dangerous avalanches with fracture heights of several

ten centimetres the minimum continuous area of this thin weak and highly deformable layer or layer-interface has to reach several hundred square meters.

The distribution of the new overburden snow, the slope angle, the local geometry of the old snow surface, snow depth, obstacles penetrating into the snow pack, and the deformability of the interface determine the stress and strain distribution along the weak layer. Locally reduced depths of the snow below the weak layer caused by irregularities of the ground surface or local densification of the new-snow slab by wind action are typical examples that generate local increases of shear strain-rate within the weak layer. At locations of increased strain-rate a process called strain-softening that can be modelled using weakest link theory (Gubler and Bader, 1989) may eventually lead to local structural collapses. The high relative motion of the grains within the super-weak zone avoids a fast renewal of stress-conducting bonds. We call this first step of failure initial fracturing. Measurements of infrasonic acoustic emissions caused by local structural collapses allow to estimate the sizes of initial fractures and their rate of occurrence. Calculations show that the typical size of initial fractures is subcritical with respect to the minimal size of super-weak inclusions necessary to initiate shear fracture propagation. To reach the critical size, several nearby initial fractures may have to coalesce to a larger superweak area. The probability of coalescence increases with increasing rate of formation of initial fractures. Measurements often show increases of the rate of acoustic emissions prior to natural avalanche releases supporting the above hypothesis (Gubler, 1980). Shear-strain concentrates within, shear stresses at the lateral border of these super-weak inclusions. If critical fracture-strain $\dot{\epsilon}$ (Fukuzawa and Narita, 1992) is attained along part of the border line fracture propagation may be initialized. The smaller the critical size L of the super-weak inclusion to start fracture propagation the more likely is its formation. The critical size L scales with slab thickness, D, and thickness of the weak-layer, d, and is inversely proportional to the geometric mean of total deformation speeds within the slab, u_s, and within the weak layer u_w (Fig.1).

$$L = const\ D\ \frac{\dot{\epsilon}_c}{\frac{1}{d}\sqrt{u_s u_w}}$$

$$u_s \propto \frac{d}{\eta_s}\tau$$

$$u_w \propto \frac{D}{\eta_w}\tau$$

τ is the asymptotic shear stress, η_s and η_w the viscosities of slab and weak layer. To get small critical L's, deformation speeds for the slab, u_s, and the weak layer, u_w, should be large and of comparable value. A very stiff slab (hard slab) or a high friction shear layer increases L significantly. A stiff slab reduces the ratios of peak to mean strain rate in the super-weak zone and of peak to mean shear stress at the border of the super-weak zone. High friction in the weak layer decreases strain rate at the boundary of the super-weak layer. From the equations it can be

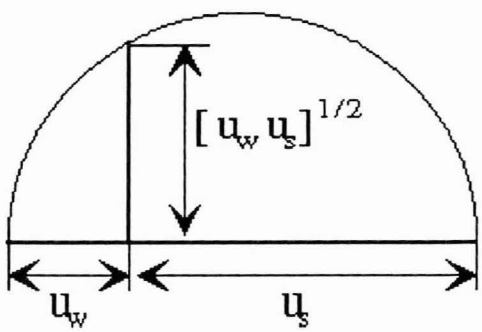

Fig. 1 Geometric mean of deformation speed for slab u_s and weak layer u_w.

seen that the weak layer should be thin, the viscosities should be small and $\eta_s \approx (D/d)\eta_w$. Because L is much larger than typical sizes of initial fractures, an additional condition for fracture propagation is the coalescence of initial fractures to a super-weak zone of minimum size. This process of coalescence is often unlikely to happen naturally. This seems a main reason for the large time scatter of natural slab avalanche releases under similar conditions. Coalescence may be triggered artificially by locally increased stresses from skiers or areal stress increases from explosives.
If a well defined weak layer exists to guide shear fracture, brittle shear-fracture (primary fracture) may propagate through areas of higher stability with respect to initial fracture. This follows because strength and critical strain are lower at the high strain rates that occur at the tip of a fast propagating fracture.

The size of a slab is limited by the extent of the weak zone, by the slope angle responsible for asymptotic shear stresses and by obstacles or snow patches of lower deformability that locally support the slab. Packed snow under tree crowns or wind packed snow may interrupt weak layers and support the slab. Sometimes shear fracture propagates through areas where the overburden slab does not move and connects isolated, but simultaneously starting slabs.

From experience it is obvious that under natural conditions the variability of local stability is often large. Therefore a few ski traces on a slope do not guarantee low avalanche danger neither does a local test with explosives. Only release-area wide tests allow for a conclusive assessment of stability or danger in case no avalanche was triggered. The above theory explains the reasons for this conclusion.

ESTIMATION OF SHORT WAVE ABSORPTION IN A SEASONAL ALPINE SNOW COVER FROM ALBEDO MEASUREMENTS.

In early and mid-winter snow-covers weak layers often form close to or at the surface of the snow-pack by recrystallization processes prior to a snow fall. Recrystallization and melt close to the snow-surface are driven by the energy exchange between snow and atmosphere. Under clear sky conditions the most important components are short-wave absorption in the snow close to the surface and long-wave emission from the snow surface.

On a typical February day, under clear sky conditions with only little wind, incoming short wave flux on a horizontal plane at the study plot of SFISAR (9°48'37" East, 46°49'50"North, 2500 m a.s.l.) near Weissfluhjoch peaks at about 600W\m^2. With an integral albedo of 0.8 120W/m^2 are absorbed in the snow. Depending on the extinction coefficient of snow about 50 to 70% of the downward net flux is absorbed within the uppermost 10mm of the snow cover. Absorption depends on snowtype, snowdensity, contaminants and the spectra of incoming radiation. Typical values for the coefficient of absorption are in the range of 50 to 90m^{-1}. Under these conditions global radiation balance of the snow-cover at noon equals zero or is slightly positive (snow pack gains energy) at a surface temperature of about -5°C. The corresponding long-wave balance at the snow surface amounts to about -115W/m^2. At low wind speeds (<3m/s) sensible and latent heat exchange between snow and atmosphere are negligible. During the night a long-wave radiation balance of -200W/m^2 cools the surface down to typically -20°C. During the day the upward heat flux in the snow very close to the surface amounts to about 100W/m^2, most of it in form of exchange of latent heat between the snow grains. Local temperature gradients in the pores between adjacent grains have to be of the order of 100°C/m

to maintain the necessary vapour flow between the grains. The rate of the corresponding recrystallisation amounts to the order of $0.1 kg/m^2h$, a very high value. These very high rates of recrystallization are responsible for fast metamorphism of near-surface snow and possibly weak layer formation. Another mechanism is surface hoar caused by water vapour saturation at a surface that has been cooled down significantly below air temperature as the result of a negative radiation balance. The shape of the ice crystals in the snow pack, bonding between the crystals and intergranular structure depend mainly on crystal growth rate and temperature. At high growth rates, corresponding to high excess vapour densities at the surface of growing crystals, facetted crystals evolve. The shape of the growing crystals, cups, plates or prism, depends on its temperature.

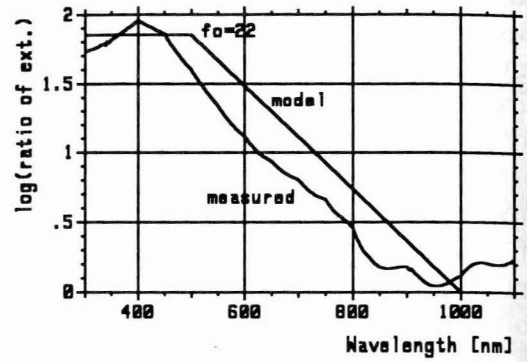

Fig. 2 Ratio of measured spectral absorption of impure ice to absorption of pure ice and the corresponding model for $f_0=22$.

To understand and model recrystallization processes close to the snow surface, radiation heating has to be known. Radiation heating depends on spectral absorption. Absorption of snow is a function of grain size, snow density, the absorption coefficient of pure ice and the amount of contamination in the granular ice with minerals or soot.

In the visible and NIR very small amounts of contaminations (O(ppmw)) increase the effective absorption for impure ice by a factor of 10 to 50 compared to pure ice. The reason for this significant increase is the very high transparency of clean ice in the visible range contrary to high absorption in the IR range. Therefore a method is needed to determine the effective short-wave absorption of near-surface snow.

Estimating Short-Wave Extinction

The goal is to determine net short-wave absorption in the snow close to the surface from quantities that can be operationally measured by sensors of automatic remote weather stations. It is assumed that contaminants are evenly distributed within the uppermost 2cm of the snow pack. This is a valid assumption as long as major input of contaminants to the snow cover happens in form of contaminated precipitation. Quantities that are relatively easy to measure automatically at a remote site are the integrated short wave albedo, snow-surface temperature, a snow temperature profile and snow depth. A concept is proposed to estimate absorption of net radiation flux in the snow close to the

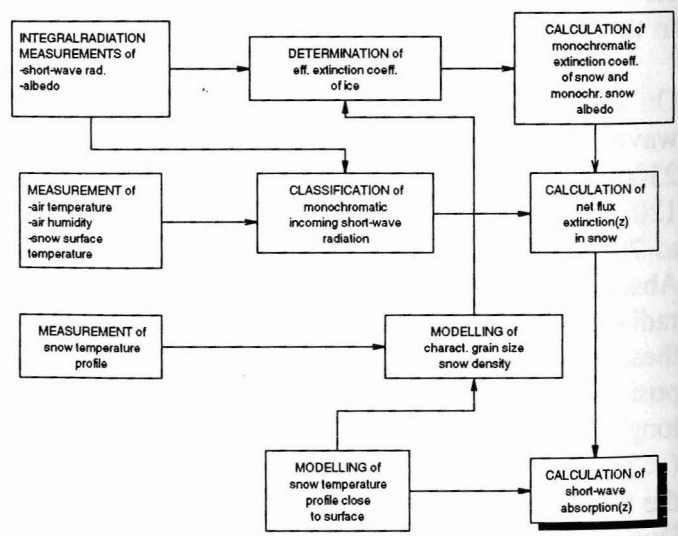

Fig. 3 Proposed steps for determinimg absorption from integral albedo measurements.

surface from these measurements. The idea is to match the measured integral albedo with a modelled albedo. The corresponding modelled albedo results from the integration of the theoretical spectral albedo weighted with spectral sensitivity of the short-wave radiation sensor in use. The theoretical spectral albedo is varied as a function of the amount of contaminants in the snow until measured and modelled integral albedo match. Spectral albedo and spectral absorption depend on the same parameters and therefore absorption can be calculated from albedo if snow density is known. Common parameters are grain size and spectral absorption of ice. Grain diameter for near-surface snow has to be determined independently. It remains to model the effect of contaminants on the absorption of ice and to vary the amount of typical impurities in the snow-model until the integral of spectral albedo matches measured integral albedo. This method is feasible if a simple 1-parameter relationship between spectral absorption of pure snow and absorption of contaminated snow exists. An approximate relationship has been found and is shown in Fig. 1.

Pure ice shows very little absorption below 600nm contrary the common contaminants are very absorptive for these wavelength. For wavelength above 1000nm pure ice is very absorptive consequently small amounts of contaminants do not increase total spectral absorption significantly. Accordingly albedo measurements and modelling can be restricted to wavelength below 1100nm.

For the calculation of the integral albedo (300 to 1000nm) and radiative heating (absorption of light) with depth, the spectral distribution of the incoming short wave radiation has to be known approximately. A classification of spectral distributions for the incoming solar radiation is possible based on the difference of snow-surface- and air temperatures (they are related to nebulosity and turbidity of the sky), incoming short wave flux, date and time (zenith angle). The flow diagram in Fig.3 visualizes the proposed steps for the determination of net flux extinction close to a snow surface.

Measurements

The measurements are performed at the study plot of SFISAR near Weissfluhjoch. A snow temperature profile with a vertical resolution of 0.1m, snow-surface temperature (Testo Therm 8400 IR-thermometer), air-temperature, air-humidity and radiation are measured and logged with a time resolution of 30 minutes. Short and long wave radiation are sampled with different instruments that have been specialy prepared to avoid snow accumulation on top of them (2-component pyranometers type S2, net pyradiometers type S1 from Swissteco; Si-photovoltaic pyranometer, Li-cor type 2000SA). The input sample rate is $1s^{-1}$, the input data are averaged for the logging period. The pyranometers are calibrated against instruments of the World Radiation Centre at Davos (WRC). For the short-wave albedo and flux measurements we recommend the use of silicon photovoltaic detectors (Li-cor Pyranometer). This type of pyranometer has the advantage to being sensitive only between 0.3 and 1.1μm. This is also the range of highest dependence of the spectral absorption of ice on impurities. Also riming of the upward looking Teflon-diffusor of the semiconductor instrument is much less of a problem than for the glass domes of full range pyranometers because of the lower IR emissivity of Teflon compared to glass and the smaller size of the instrument. A disadvantage is the dependence of the flux measurements on the spectral distribution of the incoming and reflected short-wave flux. Fortunately the albedo measurements with the semiconductor instrument depend less on sky conditions (nebolosity and turbidity) than for pyranometers with glass domes and reflect mainly the conditions of the near-surface snow. This follows from the fact that the semiconductor

instrument is only sensitive in the spectral range of high snow albedo below 1μm. Consequently the albedo measurement are less sensitive to significant changes of the relative spectral radiation fluxes in the visible and the NIR as a function of nebulosity and turbidity.

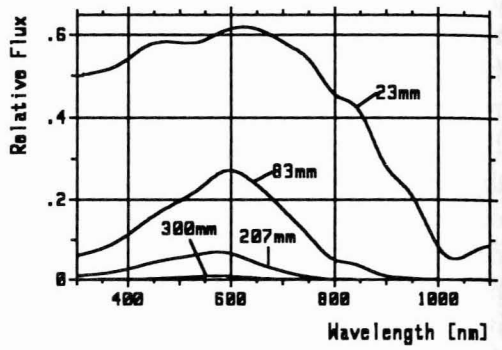

Fig. 4 Net downward flux mesured at different depth. NIR radiation is completely absorbed close to the surface.

The spectral measurements have been performed with a Li-cor portable spectrometer LI-1800 mainly using the remote cosine receptor (type 1800-11). This small sized remote receptor is connected with a fiberoptic cable to the spectrometer and therefore allows for measurements in small holes within the snow cover. The spectral range of the instrument is 300-1100nm at a spectral resolution of 6nm. This instrument is well suited for field measurements. Unfortunately the variation from true cosine response is significant for the remote sensor for zenith angles larger than 45° and has to be corrected for.

For the measurements horizontal holes were punched from a trench into the snow. The holes had a length of about 350mm and a diameter of 25mm to fit the remote cosine receptor. The diffusor of the receptor was kept in light contact with the snow during the measurements. Recordings were made with the sensor lookin upward and downward at depths between 0 and 300mm.

Net spectral downward flux J(z) is calculated by subtracting measured upward flux from downward flux. Net downward flux at different depth devided by downward flux at z=0 (surface, z-axes downward positive) is shown in Fig.4. The spectral absorption coefficient e(λ) of snow is calculated from

$$e(\lambda, z, \Delta z) = -\frac{1}{\Delta z} \ln \frac{J(\lambda, z+\Delta z)}{J(\lambda, z)}$$

J(z) was measured for z-values between 10 and 300mm. e(λ,z,Δz) is evaluated for several combinations of the z and Δz values. The corresponding snow profile is given in Fig 5. To date not enough data are available to elaborate systematic and significant dependencies of e(λ,z,Δz) on z and snow texture. Nevertheless some trends can be seen: The spectral absorption is largest close to the surface and decreases slightly with depth at least for wave-lengths between 400 and 800nm. Absorption again increases at depth between 200 and 300mm possibly due to an increase of density. The variations are within a factor of 2.

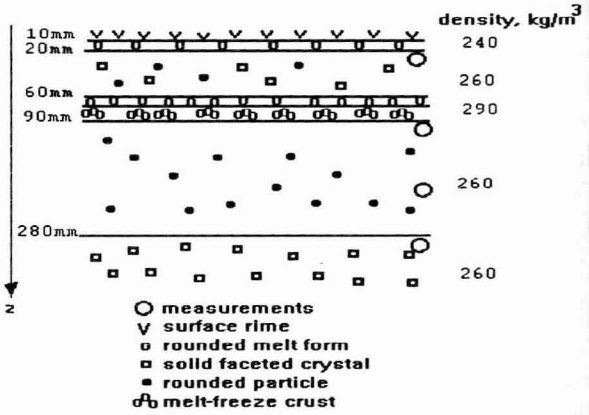

Fig. 5 Snow profile during the measurements.

The measured absorption of snow in the visible

range equals about 3 to 7 times the theoretical absorption for pure snow . We used the mixing equation for complex dielectric constants (Choudhury et. al., 1981) to estimate the order of magnitude for contaminations with either soot or minerals. This increase of absorption corresponds to an estimated pollution of the snow with either 0.1ppmw of soot or 5ppmw of minerals. The latter is more likely because deposits of Sahara dust were observed.

Typical sequences of integral albedo and radiation measurements are shown in Fig.6. The plots indicate two characteristic dependencies: (a) new snow increases the albedo significantly, the albedo drops with increasing time after a new snow fall because of increasing grain size, and (b) the albedo A' measured with the Si-pyranometer depends significantly less on sky conditions and zenith angle compared to the data of the full range pyranometer (A). Both dependencies are in good correspondence with theory: At least for the visible range the theories predict a decrease of albedo proportional to the square root of the diameter of the ice particles. The Si-pyranometer has its highest sensitivity for the wavelength of highest snow albedo, and its sensitivity drops off quickly with increasing wave length in the range of decreasing albedo. Therefore changes in the spectral distribution of the incoming solar radiation do to variing athmospheric conditions have only a minor effect on this type of albedo measurements. Both instruments show non-perfect cos-dependence for zenith angles close to 90°. Part of the increase of the recordings with the conventional pyranometer S2 is do to increasing albedo at high zenith angles because of decreasing probability of photon absorption at grazing angles of incident light. Additionally the relative high importance of diffuse light at sunrise and sunset with spectral distributions peaking at shorter wave lengths then for direct light increases the S2-albedo A too (Warren, 1982). The conventional pyranometer S2 shows a significant drop in the albedo A for increasing turbidity because of the relative increase of NIR radiation at wavelengths above 0.8μm, in the range where the spectral snow albedo a(λ) drops off in the mornings of 1/21 and 1/22. The measured albedos are lower than theoretical values for pure snow and an estimated range of grain sizes. Often the measured albedos A (.3-3μm) as well as A'(.3-1.1μm) are too low compared to theoretical values for snow consisting of pure ice and an estimated range of grain sizes. This is in good correspondence with measurements of increased extinction in near-surface snow for the same situation. As an example the Si-albedo A' during the absorption measurements mentioned above was 0.83, the estimated

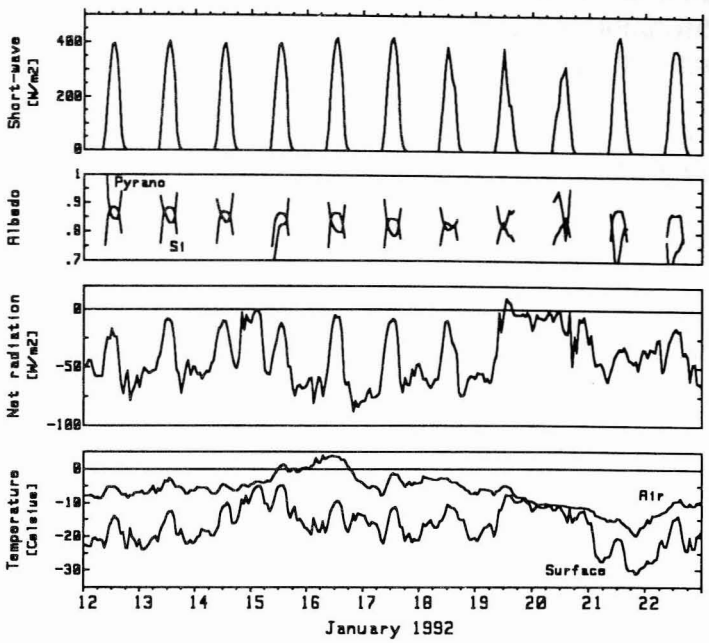

Fig. 6 Measurement of radiation, albedo and temperature for a typical winter period with clear sky coditions (1/12/92 to 1/17/92 and 1/21/92 to 1/23/92). Slight snowfall 1/10/92 and during the night 19th to 20th. Cloud covered sky is shown by approx. match of air- and surface temperature. New snow increases albedo. Grain growth decreases albedo.

grain size .5 to 1mm corresponding to an increase of absorption of ice in the visible range by more than a factor of 10 .

Application of the Method

For the determination of the extinction coefficient only typical snow albedos measured at zenith angles below 70° should be taken into account. At higher zenith angles the albedo depends on the sun-angle and also instrumental errors may be significant.

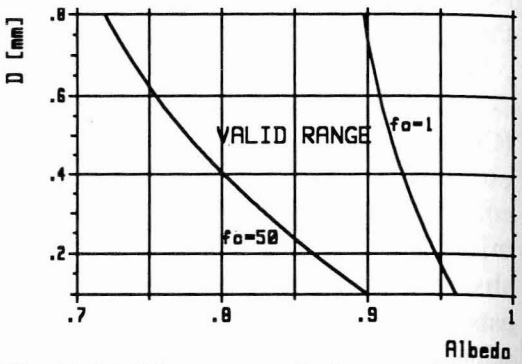

Fig. 7 Valid range of the model for moderate contaminations.

In a first step any measured combination {albedo, grain diameter} has to be tested for its validity. Acceptable values have to be within the valid range shown in Fig.7. If this condition fails either the albedo measurement or the determination of the corresponding characteristic grain size is inaccurate. A frequent reason for the former is snow or rime on the pyranometer. The grain diameter has either to be estimated from field observations or can be modelled using grain growth functions as proposed by Brun (1992). 2. the model parameter f_0 is determined by matching theoretical albedo to measured integral albedo. 3. knowing f_0 the spectral effective absorption coefficient of ice can be determined. In a last step radiation heating is calculated in function of depth by either applying the delta-Eddington method to calculate the radiation fluxes or the analytical equations for spectral albedo and absorption coefficients of snow (Choudhury, 1981). The radiation fluxes in the snow depend additionally on snow-density, grain size, and incoming monochromatic solar radiation. Snow density can be estimated using settling equations. Incoming radiation flux is measured, and its spectral distribution can be estimated as mentioned earlier.

The method described allows to improve mass and heat flow modelling in near-surface snow layers. The necessary input parameters can easily be measured at remote sites. Our measurements and experience shows that snow is often contaminated either with minerals or soot. Very small amounts of impurities significantly lower albedo and increase radiative heating close to the surface. Heat and mass flows drive the recrystallisation processes responsible for weak layer formation. Currently the method is included in our energy and mass flow model DAISY (Bader, 1992). More spectral measurements of radiation fluxes in the snow in function of snow parameters as density, grain size and shape and surface riming are necessary to further improve the model. Additional measurements are planned for winter 92/93.

CONSTITUTIVE PROPERTIES OF SNOW

Measurements of failure properties of snow by Narita (1983) as well as different types of field measurements and observations support the idea that snow will initially fail ductile. According to Narita, with some extrapolation to lower snow densities and temperatures typical of snow layers involved in direct-action avalanches, the mechanisms that determine tensile and approximately also shear strength of snow as a function of strain ϵ and strain-rate $\dot{\epsilon}$ may be subdivided into four distinct ranges (Fig.8): viscous behaviour without failure for $\dot{\epsilon} < 2 \cdot 10^{-6}\ s^{-1}$, viscoplastic deformation with incomplete macroscopic failure at large strains for $\dot{\epsilon} = 2 \cdot 10^{-6}$

$-8 \cdot 10^{-5} s^{-1}$, ductile failure for $\dot{\epsilon} = 8 \cdot 10^{-5}$ $-3 \cdot 10^{-4} s^{-1}$ and at least partly brittle failure for higher values of $\dot{\epsilon}$. Corresponding minimum strain for brittle failure is 0.1 - 0.3%, and increases with decreasing $\dot{\epsilon}$ for ductile failure from 1% to above 10%. The ratio of maximum ductile strength to minimum brittle strengths is about 2. Strengths are of the order of $5 \cdot 10^2$ to $5 \cdot 10^3$Pa. To determine these key parameters for natural weak layers, a computer controlled shear apparatus has been built and tested at SFISAR. Its transfer-area for shear stresses to the snow is $0.25 m^2$. The device allows for automatic recordings of stress, strain and strain-rate at either constant strain-rate (10^{-7} to 10^{-1} s^{-1}) or constant stress (0 to 5000Pa). The stresses are applied in situ to potential weak layers of natural snow covers. The platform is frozen to the snow a few cm above the weak layer. The platform moves itself relative to an anchor embedded in the snow pack. High sensitive deformation gauges are fixed across the weak layer to measure the strains within the weak layer. The accuracy for the stress measurements is 1Pa, for dilatations 10μm and for shear strains (10mm layer) 10^{-3}. The stress-strain rate relationships measured so far correspond to the extrapolated values mentioned above. Unfortunately critical strains for shear fracture has not yet been attained.

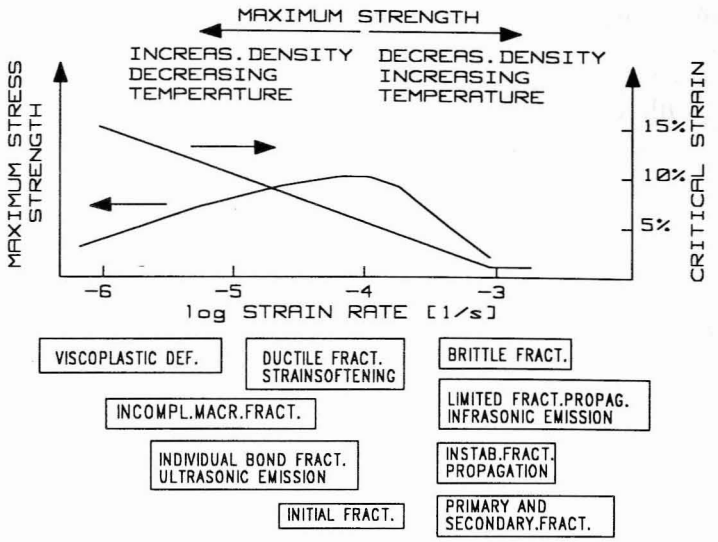

Fig. 8 Basic dependence of maximum stress/strength (arb.units) and fracture strain on strain rate.

To measure shear strain, shear and normal stress in inclined snow covers, special platforms and recording systems are used at SFISAR. With these devices we measure distortions to the stress and strain fields by trees, terraces etc., propagation of stresses caused by skiers as well as strain rates in weak layers. The data are compared to finite element calculations.

INTERCEPT EFFICIENCY AND SNOW LOSS OF SPRUCE BRANCHES

Typical subalpine spruce and larch stands near natural timberline have open canopies. The trees are arranged in groups with openings in between. Under certain conditions extreme avalanches may form in such low density stands (Gubler and Rychetnik, 1990). Their ability to prevent the formation of slab avalanches during extreme precipitation events depends partially in their ability to reduce slope parallel shear stresses in the weak layer. The backpressure zones behind obstacles protruding through the snow such as trees scales with the thickness of the slab above the highly deformable weak layer (gliding interface) but depends also on the extent of the supporting area across the slope. Any obstacle or compaction that reduces creep speed to approximately zero on a distance across the slope larger than about 3 times the slab thickness has a similar effect as an infinite wall. Rows of bushes, close standing trees or rimes of substantially compacted snow around trees with large and dense canopies are examples of natural walls. Bader et.al.(1988) finds from FE calculations:

$$\frac{x}{D} = 3 + 2.6\left(\frac{\mu_s}{\mu_w}\frac{d}{D}\right)^{0.75}$$

with x : distance of influence (95% of asymptotic value)
D : slab thickness
d : thickness of weak layer
μ_s, μ_w : viscosity of slab and weal layer

For typical ratios of the μ_s/μ_w and d/D, the distance of influence is about 3 to 4. For very weak or super-weak layers the second term gets significant, but for soft slabs the range is limited to about 10D. For isolated stems with diameters $<<$ D the zone of reduced deformation speed amounts to about 1.5D. For blocking obstacles of diameters <3D the back pressure zone reaches about 2.5D, for larger diameters an upper limit is given by the corresponding back pressure zone behind a wall. The lateral supporting range for single stems with diameters <3D is limited to 1.5D.

Below tree crowns an increased compaction during the snow fall may result from intercepted snow falling off the branches (spruce trees). For isolated spruce trees with branches reaching close to the snow surface, the snow cascading from the branches concentrates at the edge of the crown projection and causes significant compaction, even during the storm. The effect of this type of distortion depends on whether the weak layer is interrupted or not. If there is no weak layer within the compacted cross section, these portions of the snow cover effectively reduce local deformation speeds. The reduction of deformation speed, compared to the asymptotic weak layer value, depends on compaction and downslope width of the supporting zone. The corresponding stress peaks are situated well within the compacted zones. Distribution of stress and deformation around this type of support (Table 1) make it very unlikely that initial fracturing happens near the distortion.

compaction (increase of density)	downslope width of compacted zone	reduction of deformation speed at depth D	backpressure zone x/D
20%	0.5 - 4D	70 - 85%	2 - 2.7
50 - 80%	4 D	93 - 97%	2.9 - 3

Table 1 Reduction of creep speed within zones of increased viscosity (weak layer interrupted), and range of backpressure (95% limit).

It can be concluded that rims of compacted snow around the boundaries of the vertical projections of dense crowns cause by far more support to the slab than trunks belonging to permeable tree crowns. Rims are formed by 2 processes: 1. deflection of precipitation particles at intercept efficiencies <1 including knocking out of small clusters from the surface of the intercepted snow, 2. snow fall off the branches including cascading of snow specially from spruce trees. Both, internal fracture planes within the intercepted snow and sliding between snow and branch are observed. With this experiment we investigate the dependence of snow interception and snow dumping on meteorological parameters.

Experimental Setup and Results

A branch of a spruce within a group of spruces was instrumented to measure the parameters shown in Fig.9. To monitor the bending of the branch a wire attached to the branch was run vertically down to the pulley of a multi-turn potentiometer fixed to the ground. Branch deflection, snow height on the ground, mean and maximum values of temperatures, wind, air-humidity, and radiation were recorded every 30min. A geophone attached to the branch was used to trigger recordings of branch oscillations at a time resolution of 100ms. To measure surface temperature of the intercepted snow, the infrared thermometer was directed to the upper surface of the branch. The accuracy of this temperature measurement is limited by the non-ideal black-body behaviour of the snow and temperature drifts of the instrument to about $\pm 2^{\circ}C$. Branch temperature was measured with a thermistor tightly fixed to the bottom side of the branch.

Sofar the experiment has been run during five winters in subalpine forests close to natural timberline at altitudes of about 1800m a.s.l. in the region of Davos/ Switzerland, and the instrumentation has been continuously improved. During the first two winters only snow fall from trees (spruce and larch) were recorded along with meteorological parameters. For the next 3 winters the branch deflection measurement was included (spruce) and only during the last winter the IR-thermometer was added. The experiment was run on a north facing slope for the first three winters and was moved across the valley for the remaining winters. The approximate geometry of the branch instrumented during the last winter is shown in Fig.9.

To use the branch as a balance to weight the mass of intercepted snow the viscoelastic properties of the branch have to be determined. This has been done by loading the snow free branch with 20N and 50N at a given distance from the stem. Oscillations of the branch after stepwise loading and deflection during several days at varying meteorological conditions have been recorded. Bending of the branch was also modelled as a beam with variable cross section fixed at one end and loaded with point and distributed masses. This analyses allowed to determine the ultimate elastic modulus E_u of the wood of the living branch, and also to calibrate the deflection of the branch at the distance from the stem where the measuring wire was attached for different mass distributions along the branch. Fig. 10 shows typical deformation lines for different mass distributions.

The time dependence of the bending of the branch can be modelled approximately by two Kelvin-Voight-elements in series. A Kelvin-Voight model consists of a

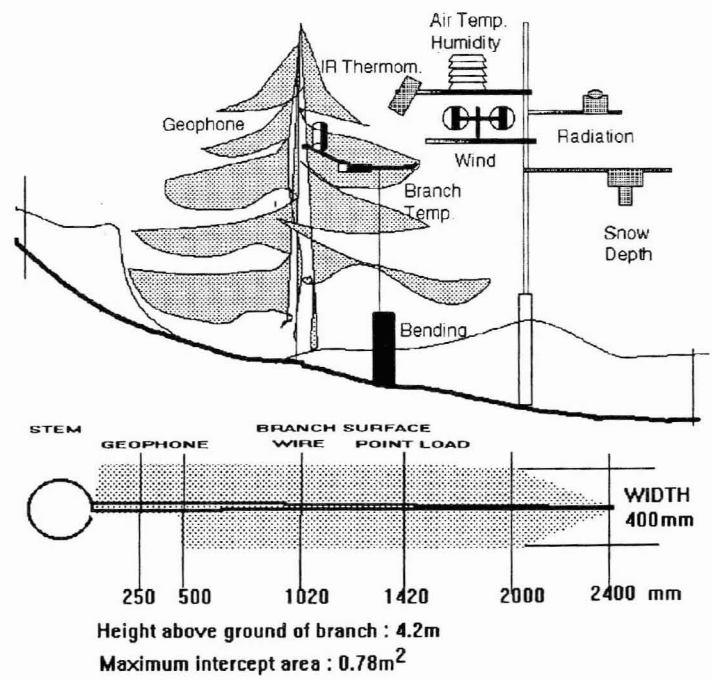

Fig.9 Instrumentation of a spruce to measure interception and geometry of the branch.

linear elastic subelement in parallel to a linear viscous subelement. Spring constant, viscosity, static and dynamic time constant for two typical mass distributions are:

measured spring constant for point loading	kp_{1stat}= 362 N/m
elastic modulus for branch wood	E = 2.4 10^9Pa
modelled spring constant using E (point load)	kmp_{1stat} = 348N/m
modelled spring constant using E (distributed load)	kmd_{stat} = 508N/m
dynamic time constant from damped oscillation	$\tau p_{1dyn} \leq$ 3.6s
viscosity of 1st KV-element from τp_{1dyn}	$\beta_1 \leq$ 8 Ns/m
corresponding static relaxation time (time to reach equilibrium deflection for 1th KV-element)	$\tau p_{1stat} \geq$ 0.022s
static relaxation time of 2nd KV-element	$\tau p_{2stat} \geq$ 3d
viscosity of 2nd KV-element (Order of magnitude)	β_2 = O(5 10^8 Ns/m)
spring constant of 2nd element (Order of magnitude)	kmp_{2stat} = O(2.5 10^3 N/m)

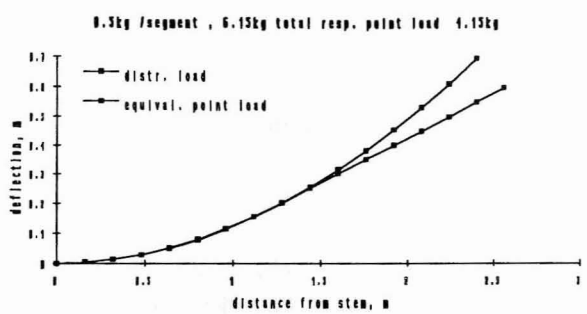

Fig.10 Bending of branch for typical mass distributions: equaly distributed load and point load at 1.02m.

The slow element (2nd) is roughly stiffer by 1 order of magnitude and has a viscosity that is 10^8 times larger compared to the fast (1st) element.

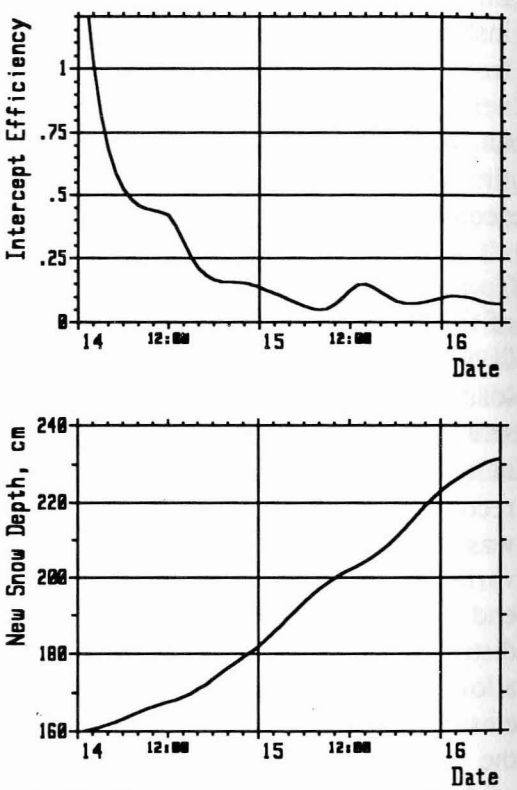

Fig.11 Intercept efficiency and snow accumulation in function of time during a typical storm.

The calibration measurements show that bending under constant load depends slightly on meteorological conditions. Measurable changes of stiffness under constant load in function of branch temperature (-5 to +5°C) have not been observed. Although the branch seems to loose weight if ventilated with dry air. These temporary decreases of deflection correspond to a loss of water of a few hundred ml (few % of estimated total weight of branch). These temporary water losses last about 6 to 12 hours and are well correlated with measured ventilation and reduced relative humidity of the air.

With the branch being calibrated as a balance three types of measurements have been performed: change of intercept efficiency during significant precipitation events, evaporation of snow from the branch, and snow dumping including melting at melting temperatures . We define intercept efficiency as the ratio of the rate of snow accumulation on the branch to snow fall intensity.

Fig. 11 shows the decrease of intercept efficiency during a storm that totalized 70cm of snow within 2.5 days. It is assumed that the relative distribution of the snow on the branch has not changed significantly during the analyzed period of time. Precipitation started on a bare branch at a precipitation rate of 0.43kg/m^2 h and an air temperature of about -5°C. Intercept efficiency was close to 100% at the beginning, but dropped to about 20% at 20cm of new snow on the ground and increasing precipitation intensity after 24hours. On the 2nd day precipitation rate increased two a maximum of 2kg/m^{2}h at a temperature around the melting point. It can be concluded that a significant amount of precipitation particles is deflected by the branches and deposits on the ground around the tree at new snow heights larger than 20 to 30cm.

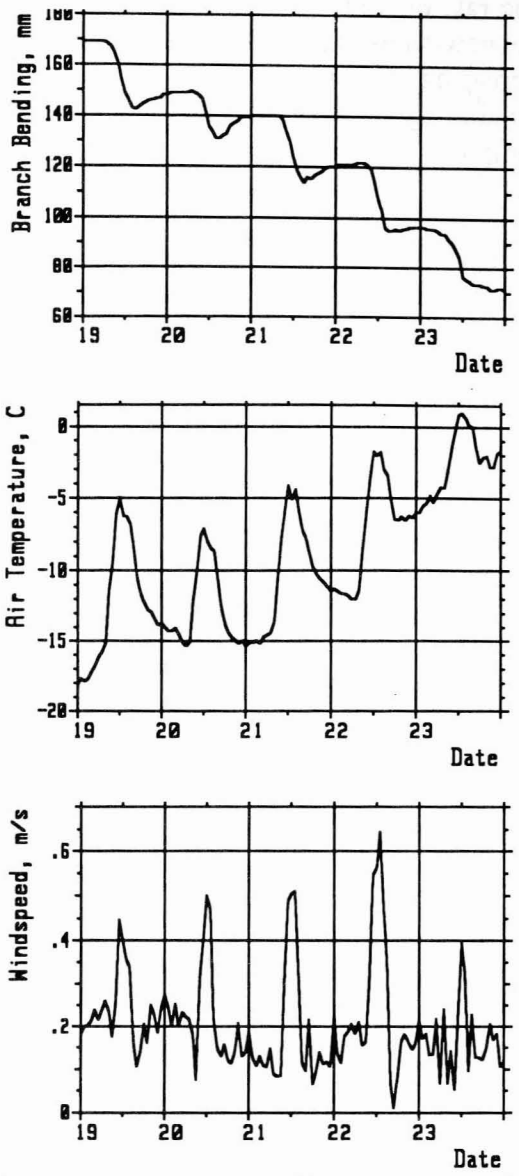

Fig. 12 Decrease of branch bending because of evaporation of snow. Air temperature and ventliation are the important parameters.

Fig.12 shows an interesting example of evaporation of snow from the branch. On several consecutive days a dry air flow ventilated the forest stand in mid morning. This air flow (.4-.8m/s, rel.humidity 40%) significantly increased evaporation of snow but obviously also water from bare needles at the bottom of the branch. Snow sublimation caused a sharp decrease of snow surface temperature on the branch although air temperature was increasing during the same period. Ceasing of air flow immediately stopped evaporation and the water content in the needles was allowed to increase again. These examples show, that at subfreezing temperatures snow sublimation from the branches results from ventilation of the dispersed snow on the branches. Ventilation of the porous snow on the branches very effectively increases latent and sensible heat transfer between snow and air. Direct and reflected solar radiation additionally input heat to the snow and even more effectively to needles from below (low albedo of needles compared to snow). Evaporation of snow from the branches between storms decreases the final snow water equivalent on the ground by up to 30% (Schmidt,1991), but also decreases the potential of snow dumping by the branch and increases the storage capacity of the branch.

The most effective process for the formation of stiffer rims around trees is snow fall or cascading from the branches. At subfreezing temperatures fracture planes normally develop within the intercepted snow. If the branch heats up above 0°C melting starts at the branch-snow interface and snow tends to slide of the branch. Fig.13 shows typical examples. At subfreezing temperature snow dumping is always induced by an increase of air temperature/ventilation as well as an increase of short wave radiation. The induced increase of snow temperature

temporarily reduces cohesion of the new snow . The rate of radius of curvature metamorphism of the new-snow particles increases significantly at increasing snow temperature resulting in a temporarily decrease of cohesion. In Fig.13 snow dumping is indicated by stepwise reduction of branch reflection, by large deflection speed measured with the geophone and resulting bending oscillations of the branch. At subfreezing temperatures only partial unloading is observed. At melting temperatures snow slides off the branches in several portions often the branch unloads completely within a short time period. It is interesting to note that substantial unloading never occurred only because of loading or intercept saturation, in all observed cases snow dumping or cascading was initialized by an increase of air temperature. In most cases increases of air temperature occur simultaneous with onset of ventilation and increases of short wave radiation . Increased rate of bending at constant load before unloading started has not been observed. Substantial unloading at subfreezing temperatures initialized by events mentioned above occurred only if the branch was recently significantly loaded close to its saturation value.

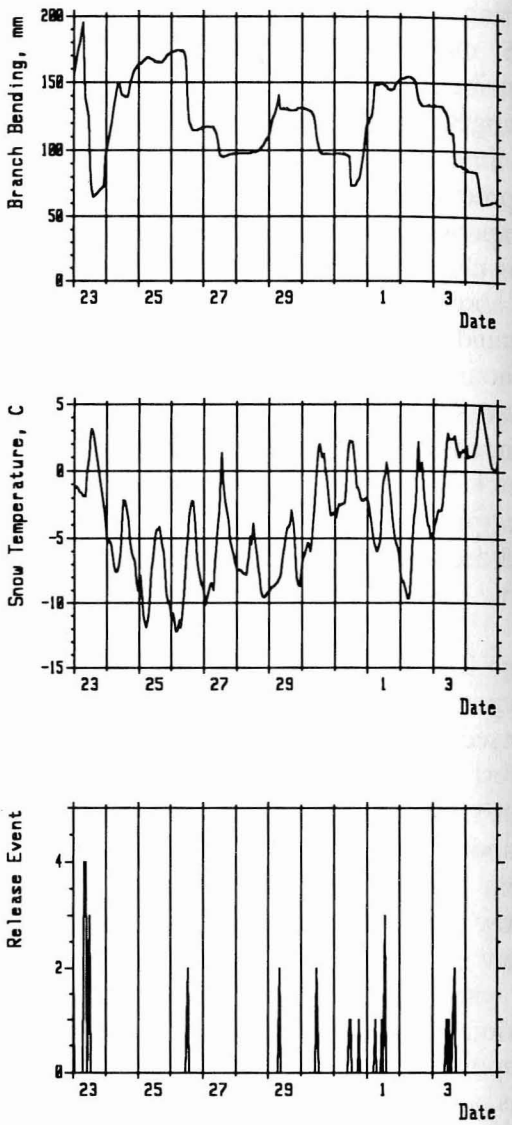

Fig. 13 Snow interception and snow fall from branch. Snow dumping caused by air temp. increase. Events of snow dumping shown on bottom graph.

CONCLUSIONS

To improve the knowledge on slab avalanche formation and prevention more specific measurements are needed to model and predict weak layer formation, to estimate the critical size of superweak inclusions and to understand avalanche formation in forest stands. Especially fracture mechanics of weak layers needs more work. The constitutive parameters of the different types of weak layers have to be determined in field experiments. Preliminary results show that the influence of snow contamination on weak layer formation may be handled in the future. During extreme and extended storms lasting several days with a potential for formation of extreme avalanches dumping of snow triggered by the daily changes of radiation input and air temperature is very likely to occur. Therefore support to the new-snow slab between the trees increases during the storm and backpressure zones of typically > 3D (D: slab thickness) form. Even clusters of spruce in an open stand may prevent formation of extreme avalanches if the maximal distance between the clusters is less than about 10m. The shape and the canopy of the spruce clusters has to be suitable for the formation of rims of compacted snow around the trees to efficiently increase support to the slab.

REFERENCES

Bader, H.P., Gubler, H.U., Salm, B. (1988) Distributions of stresses and strain-rates in snowpacks. In: Proceedings of the Sixth International Conference on Numerical Methods in Geomechanics, Innsbruck, April 1988.(ed. by G. Swoboda) p.2257-2263.

Bader, H.P., Salm, B. (1989) On the mechanics of snow slab release. In: Cold Regions Science and Technology, 17(1990) p. 287-300.

Bader, H.P., Weilenmann, P. (1992) Modeling temperature distribution, the energy and mass flow in a (phase - changing) snowpack. In: Cold Regions Science and Technology, 20(1992) p. 157-181.

Brun, E., David P., Sudul M., Brunot G. (1992) A numerical model to simulate snow-cover stratigraphy for operational avalanche forecasting. J. of Glac. Vol.38 No.128 p. 13-22.

Choudhury, B.J. 1981a. Radiative proporties of snow for clear sky solar radiation. Cold Regions Science and Technology, 4(1981) p.103-120.

Choudhury, B.J., T.Mo, J.R.Wang, A.T.C.Chang. 1981b. Albedo and flux extinction coefficients of impure snow for diffuse short-wave radiation. Cold Regions Science and Technology, 5(1981) p.119-125.

Fukuzawa T., H.Narita (1992) An experimental study on the mechanical behavior of a depth hoar layer. To be published in Annals of Glac., Proceedings of the Nagaoka Conf. 1992.

Gubler, H., Bader, H.P. (1989) A model of initial failure in slab avalanche release. In: Annals of Glaciology, Vol. 13(1989), Intl. Glac. Soc., p. 90-95.

Gubler H., J.Rychetnik (1991) Effects of forests near the timberline on avalanche formation. Proceedings of the Vienna Symposium, August 1991. IAHS Publ. no.205 p.19-37-

Gubler, H., (1980) Simultaneous measurements of stability indices and characteristic parameters describing the snow cover and the weather in fracture zones of avalanches. In: J. Glaciol. 26 (1980) 94, p. 65-74.

Gubler, H. (1992) Estimation of short wave absorption in a seasonal alpine snow cover from albedo measurements. To be published in J. of Glaciology.

Narita, H. (1983) An experimental study on tensile fracture of snow. In: Contribution Series A 25, Inst. of Low Temperature Science, Hokkaido University, Japan, p.1-37.

Schmidt, R.A., (1991) Sublimation of snow intercepted by an artificial conifer. In: Agricult. and Forest Meteorology, 54 p.1-27.

Warren, S.G. 1982. Optical proporties of snow. Reviews of Geoph. and Space Physics, Vol.20, No.1., p.67-89.